

Article

RCH₃ ··· O Interactions in Biological Systems: Are They Trifurcated H-Bonds or Noncovalent Carbon Bonds?

Antonio Bauzá and Antonio Frontera *

Department of Chemistry, Universitat de les Illes Balears, Crta de Valldemossa km 7.5, 07122 Palma de Mallorca (Balears), Spain; antonio.bauza@uib.es

* Correspondence: toni.frontera@uib.es; Tel.: +34-971-173426

Academic Editor: Sławomir J. Grabowski

Received: 26 January 2016; Accepted: 14 March 2016; Published: 17 March 2016

Abstract: In this manuscript, we combine high-level *ab initio* calculations on some model systems (XCH₃ σ-hole/H-bond donors) and a Protein Data Bank (PDB) survey to distinguish between trifurcated H-bonds and noncovalent carbon bonds in XCH₃···O complexes (X = any atom or group). Recently, it has been demonstrated both experimentally and theoretically the importance of noncovalent carbon bonds in the solid state. When an electron-rich atom interacts with a methyl group, the role of the methyl group is commonly viewed as a weak H-bond donor. However, if the electron-rich atom is located equidistant from the three H atoms, the directionality of each individual H-bond in the trifurcated binding mode is poor. Therefore, the XCH₃···O interaction could be also defined as a tetrel bond (C···O interaction). In this manuscript, we shed light into this matter and demonstrate the importance of XCH₃···O noncovalent carbon bonding interactions in two relevant protein-substrate complexes retrieved from the PDB.

Keywords: H-bonding; tetrel bonding; PDB search; *ab initio* calculations

1. Introduction

Supramolecular chemistry is a multidisciplinary field of research that develops very fast and has a deep impact [1,2] in the scientific community. Undoubtedly, the comprehension of the great deal of noncovalent forces, which are the basis of highly specific recognition, is crucial for the chemists working in this discipline. For instance, interactions between hosts and guests govern the creation of assemblies with high affinities even in highly competitive media [3–6]. For this reason, the correct description and understanding of noncovalent interactions between molecules is essential for being successful in this field of research. In general, strong and highly directional interactions, such as hydrogen bonding and σ-hole bonding [7–17], and less directional forces like ion pairing are used for this purpose.

The allocation of a hydrogen atom between a donor (D) and acceptor (A) moiety, D–H···A hydrogen bonding [18] is a particularly well studied and established supramolecular interaction ranging in strength from very weak (~1 kcal/mol) [19] to very strong (~40 kcal/mol) [20]. The weakest H-bonding interactions are established between weakly polarized D–H bonds (e.g., aliphatic CH) and mildly electron-rich H-acceptor moieties (e.g., alkene π-electrons) [21–23]. While a single interaction is energetically insignificant, when several weak H-bonds coexist they can stabilize protein structures [24–26] and contribute to the binding of proteins to carbohydrates [27–31]. Apart from this weak bonding interaction, recent theoretical explorations have suggested that pnicogen and tetrel atoms in their sp³ hybridized form can act as electron poor entities suitable to accommodate an electron-rich guest [16,32–37]. Surprisingly few studies have been dedicated to studying the most

abundant of these atoms, namely, the carbon atom. As a matter of fact, it has recently been reported that strong complexes are formed between electron-rich entities and 1,1,2,2-tetracyanocyclopropane [38–40]. Moreover, the ability of the carbon atom in a methyl group or in an aliphatic chain (sp^3 hybridized) to participate in σ -hole interactions (as a σ -hole donor, *i.e.* electron acceptor) has been explored by Mani and Arunan [41]. They demonstrated that the carbon atom in fact could act as an electrophilic center which can non-covalently bond with electron-rich entities leading to noncovalent carbon bonding, following a nomenclature analogous to other σ -hole interactions [7–17]. The theoretical predictions were confirmed experimentally by Guru Row's group [42], thus validating the existence of this type of bonding by means of X-ray charge density analysis. Electron density topologies in two prototypical crystal structures with potential carbon bonding motifs ($R_3N^+-CH_3 \cdots O/Cl$) were reported and revealed two distinct features of bond paths. That is, for the X-ray structure with the $R_3N^+-CH_3 \cdots Cl$ motif, the bond path revealed a $C-H \cdots Cl$ hydrogen bond and for the other motif the bond path connected the electron-rich oxygen atom with the $-CH_3$ carbon atom; remarkably, no other bond paths connected the oxygen atom to the $C-H$ hydrogen atoms. More recently, cooperativity effects involving carbon bonding interactions, and other noncovalent interactions have been analyzed in several theoretical studies [43–45].

The presence of methyl groups is abundant in many biologically relevant ligands and electron-rich O atoms are ubiquitous in proteins. Therefore, we wondered if perhaps weak non-covalent bonding with sp^3 hybridized carbon could have some relevance in ligand-protein complexes. Our approach was to conduct a rigorous statistical survey of the PDB together with quantum mechanical computations on the RI-MP2/aug-cc-pVTZ level of theory on some model systems. For the present theoretical study, we considered the sp^3 C-atom in several exemplifying molecules (1–3, see Figure 1) and computed their complexes with the electron-rich O atom of two molecules (formaldehyde and HO^-). In addition, using Bader's theory of "atoms in molecules" [46], we analyzed the bond path connecting the O atom with the CH_3 group in several complexes with the purpose of differentiating the H-bonding from the carbon bonding. From the PDB search, we analyzed the impact of the $X-CH_3 \cdots O$ interactions in biologically relevant protein-ligand complexes.

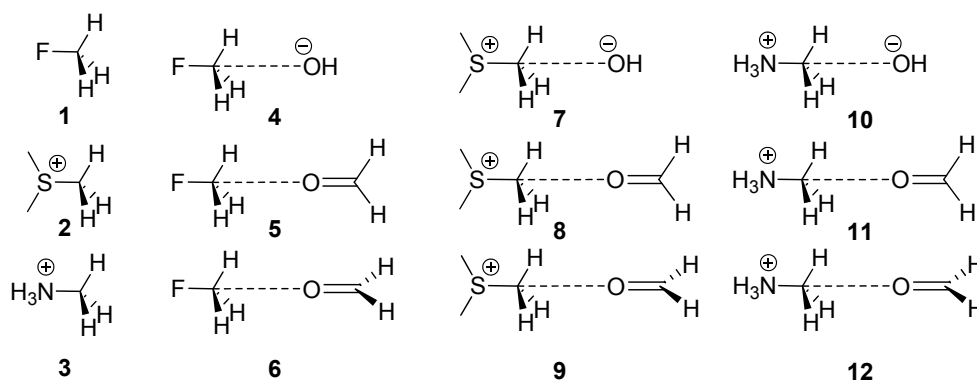


Figure 1. Compounds and complexes 1–12 studied in this work.

2. Results and Discussion

2.1. Preliminary MEP Analysis

We firstly computed the molecular electrostatic potential (MEP) mapped onto the van der Waals surface in very simple compounds (XCH_3) to explore the existence/absence of a σ -hole in the carbon atom (along the extension of the $X-C$ bond) and to compare its electrostatic potential to that measured along the $C-H$ bonds of the methyl group. In particular we computed the MEP surfaces of fluoromethane, dimethylether, dimethylthioether, dimethylformamide (DMF), acetonitrile, and methylamine, and the results are shown in Figure 2. In fluoromethane and dimethylether, an evident

σ -hole is observed (see Figure 2a,b) in the C atom with a MEP value that is comparable to that observed in the H atoms. Therefore, either the carbon or the hydrogen bonding interactions should be equally favored, at least electrostatically, in both molecules. For the DMF and acetonitrile molecules, a perfectly defined σ -hole is not observed; however, both molecules present a significantly positive value of MEP at the C atom. Finally, the methylamine and dimethylthioether molecules (see Figure 2d,e) do not present a σ -hole at the C atom, although the electrostatic potential is slightly positive. Consequently, both molecules are better H-bond donors than carbon bond donors in terms of electrostatic effects.

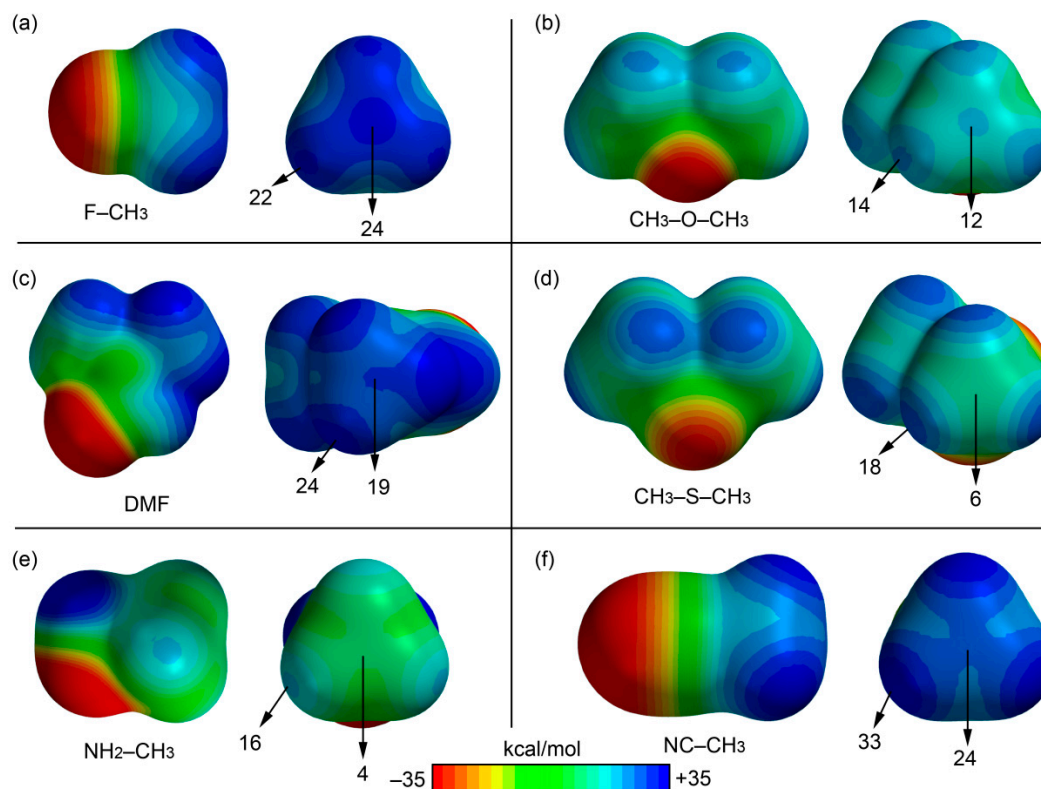


Figure 2. MEP surfaces of fluoromethane (a); dimethylether (b); DMF (c); dimethylthioether (d); methylamine (e); and acetonitrile (f). The MEP values at selected points are indicated.

2.2. Energetic and Geometric Results

Table 1 reports the interaction energies and equilibrium distances of the optimized complexes 4–12 (see Figures 1 and 3) computed at the RI-MP2/aug-cc-pVTZ level of theory. In complexes 7 and 10, where the OH[−] anion interacts with charged carbon bond donors, the noncovalent complex was not found; instead, a nucleophilic S_N2 reaction occurs in the optimization. In formaldehyde complexes, we studied the influence of the orientation of the lone pairs of the O atom on the interaction energy and equilibrium distance. At this point, it should be noted that we used two charged carbon bond donors for the following reasons. First, the utilization of trimethylsulfonium was chosen to mimic the SAM cofactor (important in methyl transfer enzymatic processes). Second, we used methanaminium because, at physiological conditions, the amine groups are likely protonated.

From the inspection of the results summarized in Table 1 and Figure 3, several points are worth discussing. First, in the fluoromethane complexes, the interaction energy with the charged OH[−] guest is large and negative (−12.9 kcal/mol), modest for the complex with the neutral formaldehyde guest (−1.9 kcal/mol). Interestingly, the carbon bonding complexes (or trifurcated H-bonded) were found to be minima on the potential hypersurface. Moreover, the orientation of the oxygen lone pairs in the formaldehyde in its complexes with fluoromethane does not influence either the interaction energy or the equilibrium distance (complexes 5 and 6). Second, the trimethylsulfonium and methanaminium

complexes with neutral formaldehyde present large interaction energies, being more favorable with the protonated amine. Third, the interaction energies are identical for both orientations of formaldehyde; however, in the case of trimethylsulfonium, the C···O equilibrium distance is longer in complex **8** than in **9** and the S–C···O angle is smaller (172.0° in **8** and 178.6° in **9**, see Figure 3b). This behavior is not observed in methanaminium complexes **11** and **12**, and both present almost identical geometric and energetic features.

Table 1. Interaction energies (BSSE corrected, ΔE_{BSSE} , kcal/mol) and equilibrium distances (R_1 and R_2 , Å) for complexes **4–12** at the RI-MP2/aug-cc-pVTZ level of theory.

Complex	ΔE_{BSSE}	R_1 (C···O)	R_2 (C···H)
4	−12.9	2.654	2.521
5	−1.9	2.993	2.829
6	−1.9	2.993	2.830
7	−1	−1	−1
8	−8.5	2.822	2.502
9	−8.5	2.803	2.665
10	−1	−1	−1
11	−9.7	2.746	2.600
12	−9.7	2.746	2.614

¹ S_N2 attack.

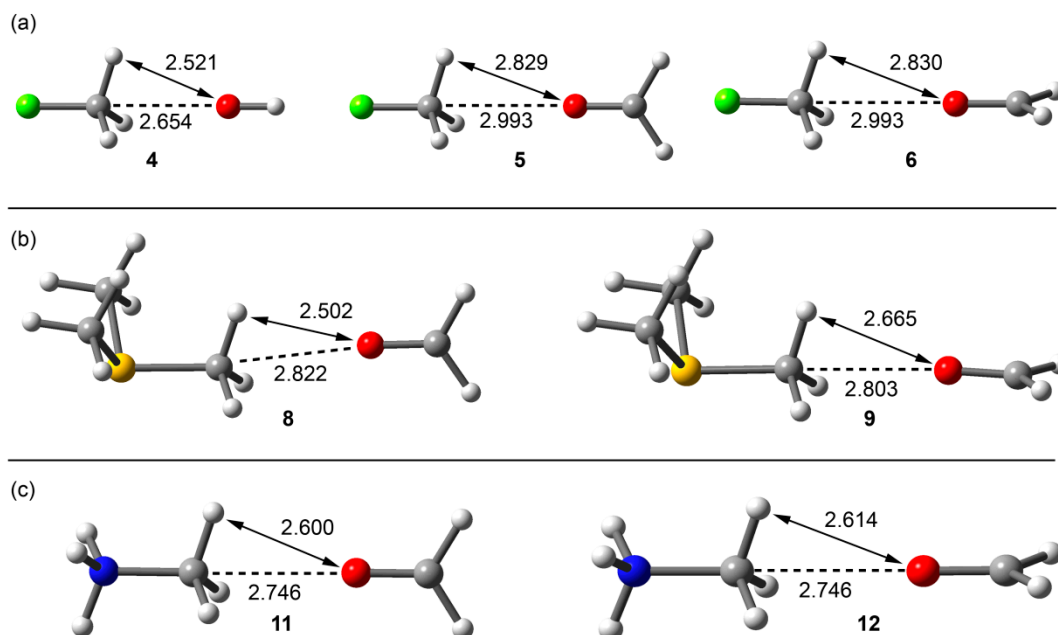


Figure 3. RI-MP2/aug-cc-pVTZ optimized complexes of fluoromethane (a); trimethylsulfonium (b); and methanaminium (c). Distances in Å.

2.3. AIM Analysis

We used Bader's theory of "atoms in molecules" (AIM) to characterize the noncovalent bonds in complexes **4–12** and to differentiate the type of interaction (carbon or hydrogen bonding). A bond critical point (CP) and a bond path connecting two atoms is unambiguous evidence of interaction. The AIM distribution of critical points and bond paths computed for the complexes is shown in Figure 4. In all CH₃F complexes (Figure 4a), the interaction is characterized by the presence of a bond CP that connects the O atom with the carbon atom, thus confirming the carbon bonding nature of this interaction. The value of ρ at the bond CP that emerges upon complexation is larger in complex **4**

than in either complex **5** or **6**, in agreement with the interaction energies and equilibrium distances. In trimethylsulfonium complex **9**, where the S–C···O angle is close to 180° , the AIM analysis shows a bond CP and bond path unambiguously connecting the C and O atoms. In complex **8**, where the S–C···O angle is 172° , the bond path presents a different trajectory and, at first sight, seems to connect the O atom of formaldehyde to the C–H bond critical point. However, a closer look reveals that the bond path suddenly deviates when it reaches the C–H bond critical point and finally connects to the C atom. The distribution in methanaminium complexes **11** and **12** (see Figure 4c) clearly shows a bond CP and bond path connecting the C and O atoms, thus confirming the carbon bonding nature of the interaction. In all cases, the Laplacian of ρ at the bond CP that connects the O and C atoms is positive, as is common in closed shell interactions. Interestingly, for the whole series of complexes, the value of ρ strongly correlates with the interaction energies. Therefore, the value of ρ can be used as a measure of bond order in this type of noncovalent bonding.

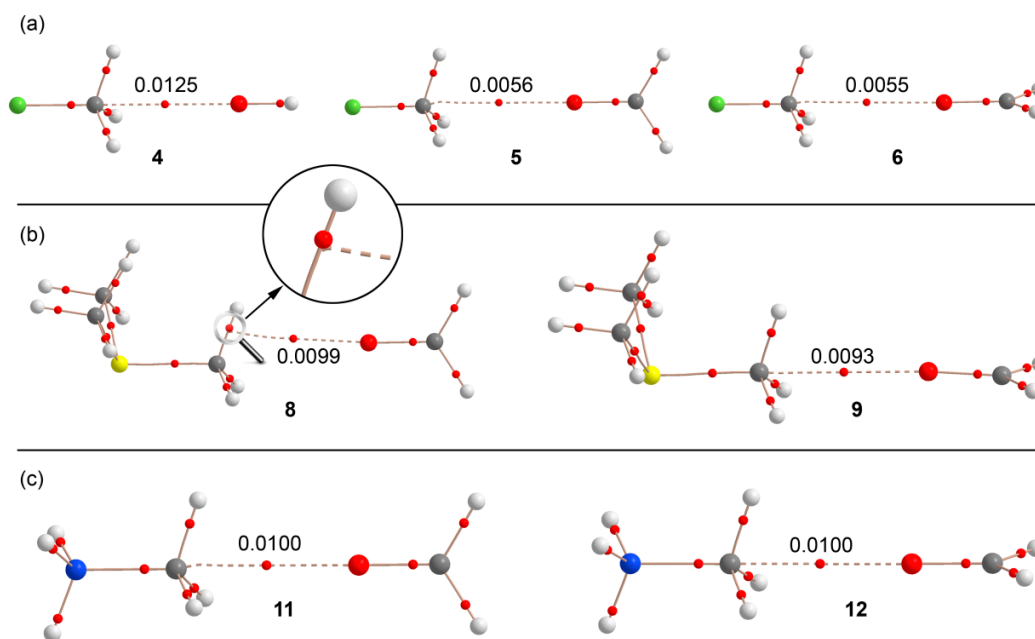


Figure 4. Distribution of critical points (red spheres) and bond paths for complexes of fluoromethane (a); trimethylsulfonium (b); and methanaminium (c) at the RI-MP2/aug-cc-pVTZ level of theory. The value of the charge density (ρ) at the bond critical points that emerge upon complexation are indicated in a.u.

We also analyzed the effect of the X–C···O angle on the interaction to find the value that causes a change from carbon bonding to hydrogen bonding. For this study, we progressively changed the F–C···O angle (α) starting from 180° and moving the O atom in two opposite directions (see Figure 5a): (i) toward a single H atom ($\alpha < 180^\circ$ values) and (ii) toward the middle of two H atoms ($\alpha > 180^\circ$ values). In each point, we optimized the geometry and simply froze the angle to the desired value. Moreover, we analyzed the distribution of critical points in order to find the value of α where the interaction changes from carbon to hydrogen bonding. If the OH^- moves to a single C–H bond (Figure 5b), the interaction rapidly changes from carbon bonding to hydrogen bonding; therefore, the critical angle is close to 170° . This result agrees with the behavior observed for complex **8** (see Figure 4) that presents an S–C···O angle of 172° , and the bond path trajectory reveals that it is in the borderline between both interactions. When the OH^- moves to the opposite direction (toward the middle of two C–H bonds), the behavior is different: For $\alpha = 190^\circ$ a bond path connects the C and O atoms similarly to fully optimized complex **4**. Curiously, and for $\alpha = 200^\circ$ and 210° , two bond paths connect the C and

O atoms, forming a bifurcated carbon bonding. As a consequence, a ring CP (yellow sphere) is also generated. Finally, at 220° , the carbon bonding changes to a bifurcated H-bonding interaction.

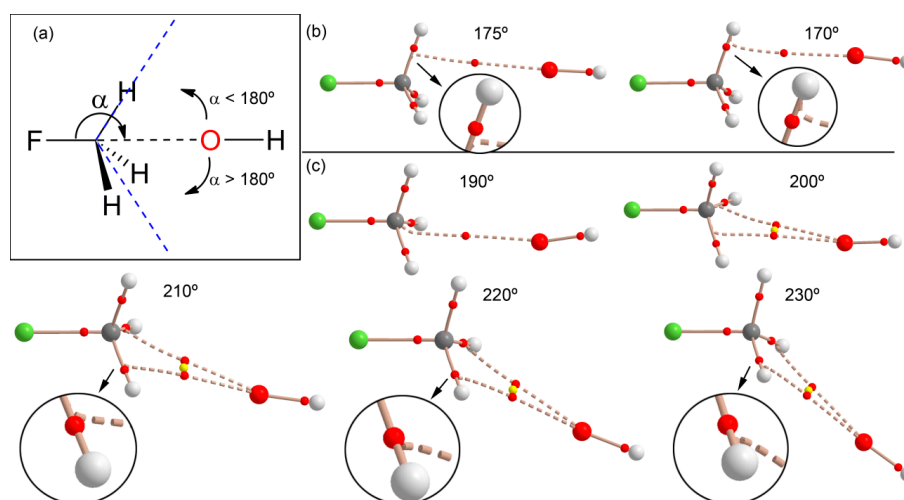


Figure 5. (a) Schematic representation of the angle and both directions; (b) distribution of critical points (red spheres) and bond paths for complexes of fluoromethane with OH^- using $\text{F}-\text{C}\cdots\text{O}$ angles $<180^\circ$ at the RI-MP2/aug-cc-pVTZ level of theory; (c) same as (b) but using angles $\alpha > 180^\circ$.

This analysis is useful for defining the search criteria of carbon bonding complexes in X-ray structure databases (CSD, PDB, *etc.*). Since the H atoms bonded to C are usually not experimentally located, there is some uncertainty regarding their real position in the CH_3 group. Therefore, it is recommended that a tight criterion regarding the $\text{X}-\text{C}\cdots\text{O}$ angle (*i.e.*, $\alpha > 170^\circ$) is used when searching for this type of noncovalent carbon bonding X-ray structures.

2.4. PDB Search

We explored the PDB in order to prove the importance of carbon bonding interactions in biologically relevant molecules. The following criteria were used for the search: (i) The CH_3 donor group belongs to the ligand and the O atom is part of the protein; (ii) $\text{C}\cdots\text{O}$ distance (d) is shorter than 3.2 \AA and the $\text{X}-\text{C}\cdots\text{O}$ angle (A) $>170^\circ$; (iii) only X-ray solid state structures are considered (no NMR resolved); and (iv) a resolution factor $<10 \text{ \AA}$. The search was performed using the freely available Relibase software [47]. As a result, we found 459 protein-ligand complexes exhibiting this type of bonding (see ESI for the full list of hits and their geometrical features, Table S1). The histograms plots for the angle and distance are represented in Figure 6. The importance of this result should be emphasized since we found a large number of hits, taking into consideration the tight geometric criteria used and that only one electron-rich element was used in the search (O). Therefore, carbon bonding interaction in general has a bright future in this field and will likely become a prominent player for explaining some biological processes, either controlling or fine-tuning the binding of substrates to enzymes.

In the original manuscripts where the protein-ligand complexes were reported, the $\text{X}-\text{CH}_3\cdots\text{O}$ interaction was either overlooked or considered as an H-bonding by the original authors. We selected two examples from this search to further illustrate the importance of this interaction. For the first example [48], we selected a very well resolved X-ray structure (PDB ID: 4NSY, resolution 1.1 \AA , see Figure 7a) that is a covalent complex between a trypsin-type serine protease (lysyl endoprotease, LysC) and its inhibitor N^α -p-tosyl-lysyl chloromethylketone (TLCK). Chloromethyl ketones such as TLCK (Figure 7b) are well-known covalent inhibitors of cysteine and serine proteases [49]. Two covalent bonds are formed with serine proteases, each one to the active-site serine and histidine. Similarly, in the LysC enzyme, the TLCK inhibitor is attacked by SER194 and by nucleophilic substitution of the Cl atom

by HIS57. This covalently bonded inhibitor interacts with the other subunit by means of a noncovalent carbon bonding interaction (see Figure 7a). We constructed a model to energetically evaluate this interaction. We substituted the SER193 and HIS47 that are covalently bonded to the inhibitor by C–H bonds in order to keep the size of the system computationally approachable. The model also includes the alanine residue and part of the peptide backbone (see Figure 7c). The interaction energy is -1.8 kcal/mol that is similar to that obtained for neutral complexes 5 and 6 (see Table 1). Remarkably, the distribution of CPs shows a bond critical point and a bond path connecting the O atom of the amide group to the carbon atom of the inhibitor, thus confirming the existence of the carbon bonding interaction in 4NSY.

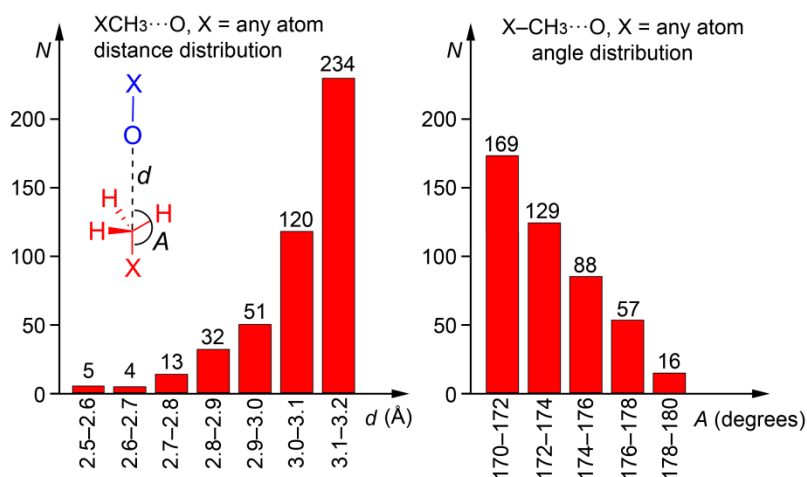


Figure 6. Histograms obtained directly from the Relibase software. Distance distribution is shown on the left and the angle distribution on the right of the figure. Inset figure: definition of d and A parameters; the protein is represented in blue and the ligand in red.

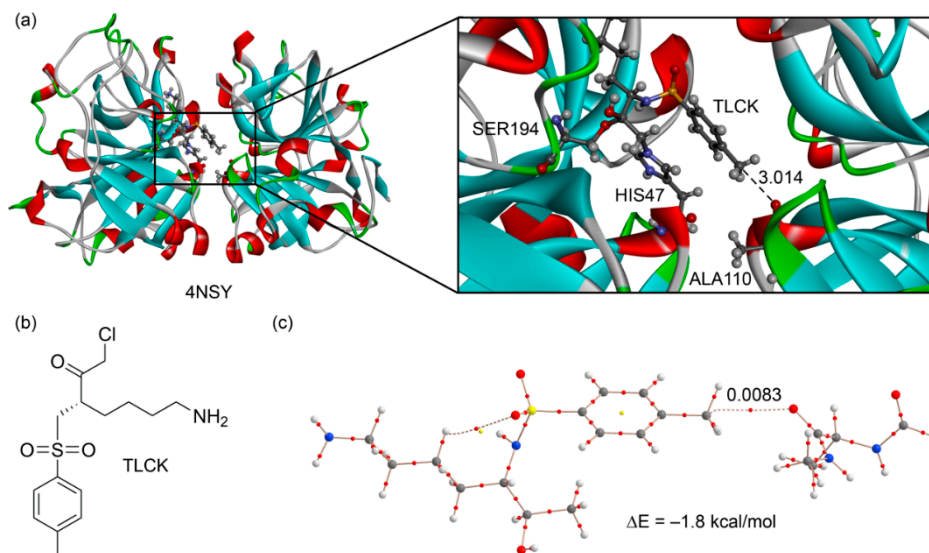


Figure 7. (a) X-ray structure of 4NSY with indication of the carbon bonding interaction (distance in Å); (b) chemical drawing of the TLCK; (c) AIM distribution of critical points of a model derived from the X-ray coordinates.

The second example we selected [50] corresponds to the structure of a M3 muscarinic acetylcholine receptor bound to tiotropium (PDB ID: 4U14, resolution 2.5 Å. see Figure 8a). Tiotropium is a

muscarinic receptor antagonist (anticholinergic bronchodilator) used in the management of chronic obstructive pulmonary disease [51]. The presence of a dimethylammonium group in the structure ensures their ability to form electrostatically assisted carbon (or hydrogen) bonding interactions using the $R_3N^+-CH_3$ groups. As a matter of fact, an aspartate residue of the active site is very close to a carbon atom belonging to one of both methyl groups (2.935 Å) with an almost linear $N-C \cdots O$ angle (177.4°). We used a theoretical model derived from the crystallographic coordinates that includes the antagonist and the aspartate bonded to a fragment of the peptide backbone. The AIM analysis confirms the existence of a carbon bonding interaction (see bond path in Figure 8a). The ASP147 residue is likely deprotonated in the X-ray structure, since both C–O distances are very similar (1.248 and 1.250 Å). In any case, we evaluated the interaction energy considering both possibilities. The interaction energy of the carbon bonding complex using the protonated ASP147 is -9.0 kcal/mol. Moreover, the value of the density at the bond critical point is $\rho = 0.0093$ a.u. These values strongly agree with those previous ones computed for methanaminium (see Table 1 and Figure 4 (complexes 11 and 12)). Considering the deprotonated ASP147, the interaction energy is very large (-73.9 kcal/mol) due to the strong electrostatic contribution. Therefore, this charge-assisted carbon bonding interaction has a strong influence on the binding of tiotropium in the muscarinic acetylcholine receptor.

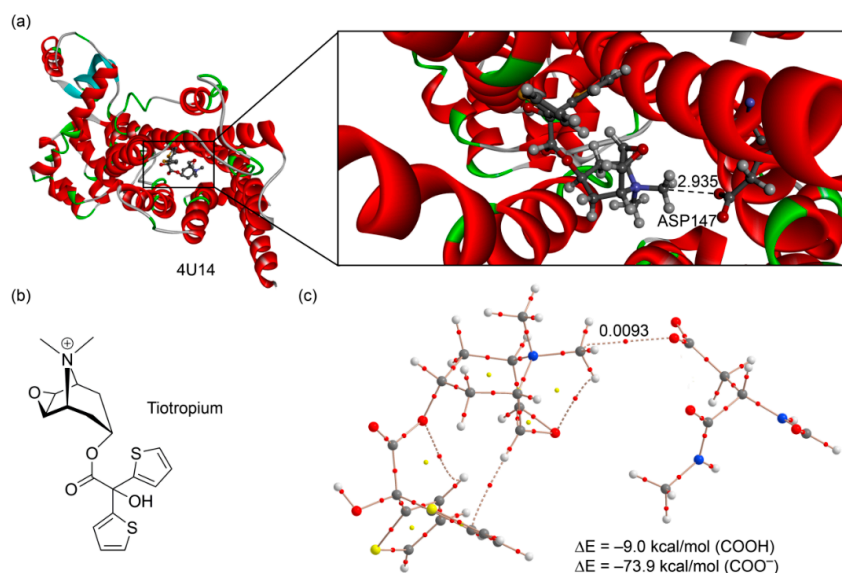


Figure 8. (a) X-ray structure of 4U14 with indication of the carbon bonding interaction (distance in Å); (b) chemical drawing of the tiotropium antagonist; (c) AIM distribution of critical points of a model retrieved from the X-ray coordinates.

2.5. NBO Analysis

To find out whether orbital effects are important to explain the carbon bonding interactions described above, we performed natural bond orbital (NBO) calculations focusing our attention on the second order perturbation analysis, due to its usefulness for studying donor-acceptor interactions [52]. We carried out the NBO calculations for complex 4 and for the theoretical model used to characterize the interaction in the PDB ID 4U14 (see Figure 8c). The results of the second order perturbation analysis are summarized in Table 2. For complex 4, we found an important orbital contribution that consists in the interaction of the lone pair orbital (LP) of the donor with the C–F antibonding orbital (BD*) of the acceptor. This interaction is significant (3.5 kcal/mol) since it accounts for approximately 27% of the total interaction energy and further confirms that the interaction in complex 4 is with the σ -hole of the carbon atom. Moreover, the expected $LP \rightarrow BD^*(C-H)$ orbital contribution that is typical of a hydrogen bond is less than 0.1 kcal/mol. Similarly, in the PDB 4U14, we found an interesting $LP(O) \rightarrow BD^*(C-N)$

contribution that is 2.0 kcal/mol and that the LP(O)→BD*(C–H) interaction is less than 0.1 kcal/mol, in sharp agreement with the AIM analysis commented above.

Table 2. Donor and acceptor NBOs with indication of the second-order interaction energy $E^{(2)}$ and donor and acceptor orbitals for complexes **4** and PDB ID 4U14. Energy values are in kcal/mol.

Complex	Donor ¹	Acceptor	$E^{(2)}$
4	LP (O)	BD* (C–H)	<0.1
	LP(O)	BD* (C–F)	3.5
4U14	LP (O)	BD* (C–H)	<0.1
	LP(O)	BD* (C–N)	2.0

¹ LP stands for lone pair orbital and BD* for antibonding orbital.

2.6. SAPT Analysis

In Table 3, we summarize the DF-DFT-SAPT energy values relative to some of the carbon bonding complexes showed above in order to show the relative importance of the electrostatic contribution to the total interaction energies, especially those involving charged carbon bonding donors. The total SAPT interaction energies for these three complexes are similar to those obtained using the RI-MP2/aug-cc-pVTZ level of theory (see Table 1), attributing reliability to the partition method and the level of theory used to compute the SAPT. The energetic contributions (Table 3) indicate that the cationic complexes **9** and **12** are clearly dominated by the electrostatic term. Moreover, the contributions of induction and dispersion terms are also important. In the neutral complex **6**, the electrostatic and dispersion terms equally contribute to the total interaction energy.

Table 3. SAPT interaction energies (E_{total} , kcal/mol) and their partitioning into the electrostatic, exchange, induction, dispersion, and contributions (E_{ee} , E_{ex} , E_{ind} , E_{disp} , respectively, kcal/mol) at the RI-DFT/aug-cc-pVTZ level of theory using the DF-DFT-SAPT approach.

Complex	E_{ee}	E_{ex}	E_{ind}	E_{disp}	E_{total}
6	−1.8	2.1	−0.2	−1.6	−1.5
9	−8.3	4.4	−1.3	−2.4	−7.6
12	−9.5	4.8	−1.7	−2.3	−8.7

To further demonstrate the importance of electrostatic forces in the interaction energies of compounds **9** and **12**, we computed the carbon bonding interaction of their equivalent neutral complexes where methylamine and dimethylthioether are used as carbon bond donors. The results are gathered in Figure 9, and it can be observed that the interaction energies are very small (−0.7 kcal/mol for **13** and −1.1 kcal/mol for **14**), in agreement with the MEP surfaces of methylamine and dimethylthioether shown in Figure 2. Moreover, the localization of the minima corresponding to the carbon bonding complexes **13** and **14** (see Figure 9) on the potential surface is worth emphasizing, since the MEP value at the H-atoms is considerably more positive than that at the C atom in both neutral molecules.

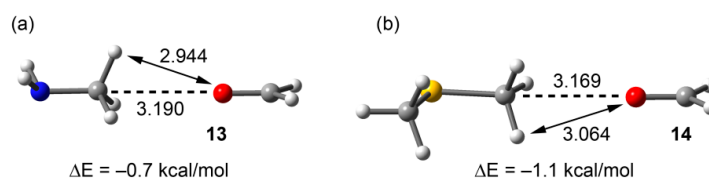


Figure 9. RI-MP2/aug-cc-pVTZ optimized complexes end interaction energies of methylamine (a) and dimethylthioether (b). Distances in Å.

3. Theoretical Methods

The geometries of the complexes studied herein have been fully optimized at the RI-MP2/aug-cc-pVTZ level of theory. Cartesian coordinates of the optimized complexes are given in the supplementary material file (Tables S2–S8). The calculations have been performed by using the program TURBOMOLE version 7.0 [53]. The interaction energies were calculated with correction for the basis set superposition error (BSSE) by using the Boys–Bernardi counterpoise technique [54]. The C_s symmetry point group has been used in the optimization of the complexes. The minimum nature of the complexes has been confirmed by carrying out frequency calculations. For the theoretical analysis of the noncovalent interactions present in PDB structures 4NSY and 4U14, the BP86-D3/aug-cc-pVTZ level of theory was used; the position of the hydrogen atoms present in these structures was optimized prior to the evaluation of the binding energy values. For the hereoatoms we used the crystallographic coordinates, we used the DFT-D functional with the latest available correction for dispersion (D3) [55]. Bader’s “atoms in molecules” theory was used to study the interactions discussed herein by means of the AIMall calculation package [56]. Finally, the partitioning of the interaction energies into the individual electrostatic, induction, dispersion, and exchange-repulsion components was carried out with the symmetry adapted intermolecular perturbation theory approach DFT-SAPT at the BP86/aug-cc-pVTZ level of theory using the aug-cc-pVQZ basis set for the MP2 density fitting [57] by means of the MOLPRO program [58,59].

4. Conclusions

In this manuscript, we analyzed the dual ability of the methyl group (XCH_3) to act as either H-bond or carbon bond donor in complexes with electron-rich oxygen atoms by means of high-level *ab initio* calculations and using Bader’s theory of atoms in molecules. For $X-C \cdots O$ complexes exhibiting angles close to linearity, a carbon bonding interaction instead of H-bonding is established as confirmed by AIM and NBO analyses. The importance of electrostatic and dispersion contributions to the interaction energy of the carbon bonding complexes was shown using the SAPT partition scheme. We demonstrated the importance of latter interactions in biological systems by examining the PDB and illustrated this in two selected examples. Since $-CH_3$ groups are commonplace, non-covalent carbon bonding involving this group might turn out to be as functionally relevant as other σ -hole and hydrogen bonding interactions.

Supplementary Materials: The following are available online at <http://www.mdpi.com/2073-4352/6/3/26/s1>. Table S1: Results from the PDB search. Distances in Å. Angles in degrees. Table S2: Cartesian coordinates of the complexes 4. Table S3: Cartesian coordinates of the complexes 5. Table S4: Cartesian coordinates of the complexes 6. Table S5: Cartesian coordinates of the complexes 8. Table S6: Cartesian coordinates of the complexes 9. Table S7: Cartesian coordinates of the complexes 11. Table S8: Cartesian coordinates of the complexes 12.

Acknowledgments: We thank CONSOLIDER-Ingenio 2010 (project CSD2010-0065) and the MICINN of Spain (project CTQ2014-57393-C2-1-P FEDER funds). We thank the CTI for computational facilities.

Author Contributions: Antonio Bauzá and Antonio Frontera conceived and designed the calculations; Antonio Bauzá and Antonio Frontera analyzed the data; Antonio Frontera wrote the paper.

Conflicts of Interest: The authors declare no conflict of interest. The founding sponsors had no role in the design of the study, in the collection, analyses, or interpretation of data, in the writing of the manuscript, or in the decision to publish the results.

Abbreviations

The following abbreviations are used in this manuscript:

AIM	Atoms in molecules
DMF	Dimethylformamide
MEP	Molecular electrostatic potential

MP2	Second order Moller-Plesset
SAM	S-Adenosyl methionine
PDB	Protein Databank
CSD	Cambridge Structural Database
CP	Critical point
LysC	lysyl endoproteinase
TLCK	N ^α -p-tosyl-lysyl chloromethylketone
ASP	Aspartate
HIS	Histidine
SER	Serine
NBO	Natural Bond Orbital
SAPT	Symmetry adapted perturbation theory

References

1. Schneider, H.J. Binding mechanisms in supramolecular complexes. *Angew. Chem. Int. Ed.* **2009**, *48*, 3924–3977. [[CrossRef](#)] [[PubMed](#)]
2. Schneider, H.J.; Yatsimirski, A. *Principles and Methods in Supramolecular Chemistry*; Wiley: Chichester, UK, 2000.
3. Lehn, J.M. *Supramolecular Chemistry Concepts and Perspectives*; Wiley-VCH: Weinheim, Germany, 1995.
4. Vögtle, F. *Supramolecular Chemistry: An Introduction*; Wiley: New York, NY, USA, 1993.
5. Beer, P.D.; Gale, P.A.; Smith, D.K. *Supramolecular Chemistry*; Oxford University Press: Oxford, UK, 1999.
6. Steed, J.W.; Atwood, J.L. *Supramolecular Chemistry*; Wiley: Chichester, UK, 2000.
7. Destecroix, H.; Renney, H.C.M.; Mooibroek, T.J.; Carter, T.S.; Stewart, P.F.N.; Crump, M.P.; Davis, A.P. Affinity enhancement by dendritic side chains in synthetic carbohydrate receptors. *Angew. Chem. Int. Ed.* **2015**, *54*, 2057–2061. [[CrossRef](#)] [[PubMed](#)]
8. Murray-Rust, P.; Motherwell, W.D.S. Computer retrieval and analysis of molecular geometry. 4. Intermolecular interactions. *J. Am. Chem. Soc.* **1979**, *101*, 4374–4376. [[CrossRef](#)]
9. Murray-Rust, P.; Stallings, W.C.; Monti, C.T.; Preston, R.K.; Glusker, J.P. Intermolecular interactions of the carbon-fluorine bond: The crystallographic environment of fluorinated carboxylic acids and related structures. *J. Am. Chem. Soc.* **1983**, *105*, 3206–3214. [[CrossRef](#)]
10. Ramasubbu, N.; Parthasarathy, R.; Murray-Rust, P. Angular preferences of intermolecular forces around halogen centers: Preferred directions of approach of electrophiles and nucleophiles around carbon-halogen bond. *J. Am. Chem. Soc.* **1986**, *108*, 4308–4314. [[CrossRef](#)]
11. Metrangolo, P.; Neukirch, H.; Pilati, T.; Resnati, G. Halogen bonding based recognition processes: A world parallel to hydrogen bonding. *Acc. Chem. Res.* **2005**, *38*, 386–395. [[CrossRef](#)] [[PubMed](#)]
12. Politzer, P.; Murray, J.S. Halogen bonding: An interim discussion. *ChemPhysChem* **2013**, *14*, 278–294. [[CrossRef](#)] [[PubMed](#)]
13. Bauzá, A.; Mooibroek, T.J.; Frontera, A. The Bright Future of Unconventional σ/π -Hole Interactions. *ChemPhysChem* **2015**, *16*, 2496–2517. [[CrossRef](#)] [[PubMed](#)]
14. Politzer, P.; Murray, J.S.; Clark, T. Halogen bonding: An electrostatically-driven highly directional noncovalent interaction. *Phys. Chem. Chem. Phys.* **2010**, *12*, 7748–7757. [[CrossRef](#)] [[PubMed](#)]
15. Bauzá, A.; Mooibroek, T.J.; Frontera, A. Tetrel Bonding Interactions. *Chem. Rec.* **2016**, *16*, 473–487. [[CrossRef](#)] [[PubMed](#)]
16. Bauzá, A.; Mooibroek, T.J.; Frontera, A. Tetrel-bonding interaction: Rediscovered supramolecular force? *Angew. Chem. Int. Ed.* **2013**, *52*, 12317–12321. [[CrossRef](#)] [[PubMed](#)]
17. Bauzá, A.; Frontera, A. Competition between halogen bonding and π -hole interactions involving various donors: the role of dispersion effects. *ChemPhysChem* **2015**, *16*, 3108–3113.
18. Desiraju, G.R. A bond by any other name. *Angew. Chem. Int. Ed.* **2011**, *50*, 52–59. [[CrossRef](#)] [[PubMed](#)]
19. Desiraju, G.R.; Steiner, T. *The Weak Hydrogen Bond in Structural Chemistry and Biology*; Oxford University Press: Oxford, UK, 1999.

20. Larson, J.W.; McMahon, T.B. Gas-phase bihalide and pseudobihalide ions. An ion cyclotron resonance determination of hydrogen bond energies in XHY⁻ species (X, Y = F, Cl, Br, CN). *Inorg. Chem.* **1984**, *23*, 2029–2033. [[CrossRef](#)]
21. Nishio, M.; Umezawa, Y.; Fantini, J.; Weiss, M.S.; Chakrabarti, P. CH– π hydrogen bonds in biological macromolecules. *Phys. Chem. Chem. Phys.* **2014**, *16*, 12648–12683. [[CrossRef](#)] [[PubMed](#)]
22. Nishio, M.; Umezawa, Y.; Honda, K.; Tsuboyamad, S.; Suezawae, H. CH/ π hydrogen bonds in organic and organometallic chemistry. *CrystEngComm* **2009**, *11*, 1757–1788. [[CrossRef](#)]
23. Nishio, M.; Hirota, M.; Umezawa, Y. *The C–H/ π Interaction: Evidence, Nature, Consequences*; Wiley: New York, NY, USA, 1998.
24. Samanta, U.; Pal, D.; Chakrabarti, P. Environment of tryptophan side chains in proteins. *Proteins* **2000**, *38*, 288–300. [[CrossRef](#)]
25. Plevin, M.J.; Bryce, D.L.; Boisbouvier, J. Direct detection of CH/ π interactions in proteins. *Nat. Chem.* **2010**, *2*, 466–471. [[CrossRef](#)] [[PubMed](#)]
26. Brandl, M.; Weiss, M.M.S.; Jabs, A.; Sühnel, J.; Hilgenfeld, R. C–H... π -interactions in proteins. *J. Mol. Biol.* **2001**, *307*, 357–377. [[CrossRef](#)] [[PubMed](#)]
27. Quioco, F.A.; Vyas, N.K. Novel stereospecificity of the L-arabinose-binding protein. *Nature* **1984**, *310*, 381–386. [[CrossRef](#)] [[PubMed](#)]
28. Vyas, N.K.; Vyas, M.N.; Quioco, F.A. Sugar and signal-transducer binding sites of the *Escherichia coli* galactose chemoreceptor protein. *Science* **1988**, *242*, 1290–1295. [[CrossRef](#)] [[PubMed](#)]
29. Nishio, M. The CH/ π hydrogen bond in chemistry. Conformation, supramolecules, optical resolution and interactions involving carbohydrates. *Phys. Chem. Chem. Phys.* **2011**, *13*, 13873–13900. [[CrossRef](#)] [[PubMed](#)]
30. Laughrey, Z.R.; Kiehna, S.E.; Riemen, A.J.; Waters, M.L. Carbohydrate– π Interactions: what are they worth? *J. Am. Chem. Soc.* **2008**, *130*, 14625–14633. [[CrossRef](#)] [[PubMed](#)]
31. Barwell, N.P.; Davis, A.P. Substituent effects in synthetic lectins—Exploring the role of CH– π interactions in carbohydrate recognition. *J. Org. Chem.* **2011**, *76*, 6548–6557. [[CrossRef](#)] [[PubMed](#)]
32. Politzer, P.; Murray, J.S.; Clark, T. Halogen bonding and other σ -hole interactions: A perspective. *Phys. Chem. Chem. Phys.* **2013**, *15*, 11178–11189. [[CrossRef](#)] [[PubMed](#)]
33. Murray, J.S.; Riley, K.E.; Politzer, P.; Clark, T. Directional weak intermolecular interactions: σ -hole bonding. *Aust. J. Chem.* **2010**, *63*, 1598–1607. [[CrossRef](#)]
34. Clark, T. σ -Holes. *Wiley Interdiscip. Rev. Comput. Mol. Sci.* **2013**, *3*, 13–20. [[CrossRef](#)]
35. Bauzá, A.; Mooibroek, T.J.; Frontera, A. σ -Hole opposite to a lone pair: unconventional pnictogen bonding interactions between ZF₃ (Z = N, P, As and Sb). *ChemPhysChem* **2016**, *17*. [[CrossRef](#)]
36. Bundhun, A.; Ramasami, P.; Murray, J.S.; Politzer, P. Trends in σ -hole strengths and interactions of F₃MX molecules (M = C, Si, Ge and X = F, Cl, Br, I). *J. Mol. Model.* **2013**, *19*, 2739–2746. [[CrossRef](#)] [[PubMed](#)]
37. Grabowski, S.J. Tetrel bond– σ -hole bond as a preliminary stage of the SN₂ reaction. *Phys. Chem. Chem. Phys.* **2014**, *16*, 1824–1834. [[CrossRef](#)] [[PubMed](#)]
38. Bauzá, A.; Mooibroek, T.J.; Frontera, A. Small cycloalkane (CN)₂C–C(CN)₂ Structures Are Highly Directional Non-covalent Carbon–Bond Donors. *Chem. Eur. J.* **2014**, *20*, 10245–10248.
39. Bauzá, A.; Mooibroek, T.J.; Frontera, A. 1,1,2,2-Tetracyanocyclopropane (TCCP) as supramolecular synthon. *Phys. Chem. Chem. Phys.* **2016**, *18*, 1693–1698. [[CrossRef](#)] [[PubMed](#)]
40. Escudero-Adán, E.C.; Bauzá, A.; Frontera, A.; Ballester, P. Nature of noncovalent carbon-bonding interactions derived from experimental charge-density analysis. *ChemPhysChem* **2015**, *16*, 2530–2533. [[CrossRef](#)] [[PubMed](#)]
41. Mani, D.; Arunan, E. The X–C...Y (X = O/F, Y = O/S/F/Cl/Br/N/P) ‘carbon bond’ and hydrophobic interactions. *Phys. Chem. Chem. Phys.* **2013**, *15*, 14377–14383. [[CrossRef](#)] [[PubMed](#)]
42. Thomas, S.P.; Pavan, M.S.; Row, T.N.G. Experimental evidence for ‘carbon bonding’ in the solid state from charge density analysis. *Chem. Commun.* **2014**, *50*, 49–51. [[CrossRef](#)] [[PubMed](#)]
43. Solimannejad, M.; Orojloo, M.; Amani, S. Effect of cooperativity in lithium bonding on the strength of halogen bonding and tetrel bonding: (LiCN)_n...ClYF₃ and (LiCN)_n...YF₃Cl (Y = C, Si and n = 1–5) complexes as a working model. *J. Mol. Model.* **2015**, *21*, 183. [[CrossRef](#)] [[PubMed](#)]
44. Marín-Luna, M.; Alkorta, I.; Elguero, J. Cooperativity in Tetrel Bonds. *J. Phys. Chem. A* **2016**, *120*, 648–656. [[CrossRef](#)] [[PubMed](#)]

45. Guo, X.; Liu, Y.-W.; Li, Q.-Z.; Li, W.-Z.; Cheng, J.-B. Competition and cooperativity between tetrel bond and chalcogen bond in complexes involving F2CX (X = Se and Te). *Chem. Phys. Lett.* **2015**, *620*, 7–12. [[CrossRef](#)]
46. Bader, R.F.W. A quantum theory of molecular structure and its applications. *Chem. Rev.* **1991**, *91*, 893–928. [[CrossRef](#)]
47. Relibase. Available online: <https://www.ccdc.cam.ac.uk/Community/freeservices/Relibase/> (accessed on 25 January 2016).
48. Asztalos, P.; Müller, A.; Hölke, W.; Sobek, H.; Rudolph, M.G. Atomic resolution structure of a lysine-specific endoprotease from *Lysobacter enzymogenes* suggests a hydroxyl group bound to the oxyanion hole. *Acta Crystallogr. Sect. D—Biol. Crystallogr.* **2014**, *70*, 1832–1843. [[CrossRef](#)] [[PubMed](#)]
49. Drenth, J. Binding of chloromethyl ketone substrate analogues to crystalline papain. *Biochemistry* **1976**, *15*, 3731–3738. [[CrossRef](#)] [[PubMed](#)]
50. Thorsen, T.S.; Matt, R.; Weis, W.I.; Kobilka, B.K. Modified T4 Lysozyme Fusion Proteins Facilitate G Protein-Coupled Receptor Crystallography. *Structure* **2014**, *22*, 1657–1664. [[CrossRef](#)] [[PubMed](#)]
51. Kato, M.; Komamura, K.; Kitakaze, M. Tiotropium, a novel muscarinic M3 receptor antagonist, improved symptoms of chronic obstructive pulmonary disease complicated by chronic heart failure. *Circ. J.* **2006**, *70*, 1658–1660. [[CrossRef](#)] [[PubMed](#)]
52. Weinhold, F.; Landis, C.R. *Valency and Bonding: A Natural Bond Orbital Donor-Acceptor Perspective*; Cambridge University Press: Cambridge, UK, 2005.
53. Ahlrichs, R.; Bär, M.; Hacer, M.; Horn, H.; Kömel, C. Electronic structure calculations on workstation computers: the program system TURBOMOLE. *Chem. Phys. Lett.* **1989**, *162*, 165–169. [[CrossRef](#)]
54. Boys, S.B.; Bernardi, F. The calculation of small molecular interactions by the differences of separate total energies. Some procedures with reduced errors. *Mol. Phys.* **1970**, *19*, 553–566. [[CrossRef](#)]
55. Grimme, S.; Antony, J.; Ehrlich, S.; Krieg, H.A. Consistent and accurate *ab initio* parametrization of density functional dispersion correction (DFT-D) for the 94 elements H-Pu. *J. Chem. Phys.* **2010**, *132*, 154104–154119. [[CrossRef](#)] [[PubMed](#)]
56. Todd, A.; Keith, T.K. *AIMAll*; Version 13.05.06; Gristmill Software: Overland Park, KS, USA, 2013.
57. Heßelmann, A.; Jansen, G. The helium dimer potential from a combined density functional theory and symmetry-adapted perturbation theory approach using an exact exchange–correlation potential. *Phys. Chem. Chem. Phys.* **2003**, *5*, 5010–5014. [[CrossRef](#)]
58. Werner, H.-J.; Knowles, P.J.; Knizia, G.; Manby, F.R.; Schütz, M. Molpro: A general-purpose quantum chemistry program package. *WIREs Comput. Mol. Sci.* **2012**, *2*, 242–253. [[CrossRef](#)]
59. Werner, H.-J.; Knowles, P.J.; Knizia, G.; Manby, F.R.; Schütz, M.; Celani, P.; Korona, T.; Lindh, R.; Mitrushenkov, A.; Rauhut, G.; *et al.* MOLPRO, Version 2012.1; a Package of *ab Initio* Programs. Available online: <https://www.molpro.net/info/authors> (accessed on 15 March 2016).



© 2016 by the authors; licensee MDPI, Basel, Switzerland. This article is an open access article distributed under the terms and conditions of the Creative Commons by Attribution (CC-BY) license (<http://creativecommons.org/licenses/by/4.0/>).